Evaporating drops on patterned surfaces: transition from pinned to moving triple line

Neeharika Anantharaju[‡], Mahesh Panchagnula[‡]* and Sudhakar Neti[†]

[‡]*Dept of Mechanical Engineering, Tennessee Technological University, Cookeville TN 38501*

**Phone: (931) 372 6143, FAX: (931) 372 6340, mvp@tntech.edu*

[†]*P.C. Rossin College of Engineering, Lehigh University, Bethlehem PA 18015*

ABSTRACT:

Evaporation of sessile drops on micro-patterned surfaces is investigated over a range of heterogeneity length scales and solid area fractions. The surface topology is generated by a uniform arrangement of square pillars or square holes. The evaporation process is captured using high resolution imaging techniques and later post-processed for such information as contact angle, contact circle diameter and drop volume. It is observed that two distinct phases of evaporation existed for all substrate characteristics: pinned triple line (TL) phase and moving TL phase. In both phases, the process follows a linear decrease of surface area. The dimensionless evaporation rate constant is found to be higher during the moving TL phase in comparison with the pinned TL phase. In addition, it is found that the triple line topology has no effect on the evaporation rate constant.

KEYWORDS: Evaporation, Superhydrophobicity, Triple line, Pinned and moving triple line.

Introduction:

Evaporation of water droplets is a fundamental phenomenon in nature [1]. The phase change characteristics associated with a sessile drop and its wettability behavior are intricately linked. Wettability of a surface is typically characterized by the contact angle that a sessile drop renders at the surface. The triple line (TL), defined as the set of points that are in contact with the solid, liquid and vapor phases, also plays an important role. The contact angle is known to be governed by the chemical composition and surface topology as well as the ability of the contact line to remain pinned on a defect. Therefore, on a non-ideal surface, this contact angle is not unique and takes on a range of values between two extrema termed the advancing (θ_a) and receding (θ_r) contact angles. It is known that the drop evaporation affects the contact angle and vice versa. The focus of this paper is to understand this relationship in the context of the triple line motion.

The evaporation of a sessile liquid drop proceeds by mass diffusion driven by concentration gradient studied herein experimentally under isothermal conditions. The atmosphere in the immediate vicinity of the drop is saturated by liquid vapor (Figure 1), while the atmosphere far from the drop is unsaturated. The rate of evaporation by diffusion depends not only on this concentration gradient but also on the instantaneous contact angle [2]. Thus a complete understanding of the evaporation process on rough surfaces as well as its effect on the contact angle is important to several industrial and biological applications.

Picknett and Bexon [3], in one of the early studies of evaporating sessile drops, observed three distinct phases of evaporation. The first is a constant contact area phase (referred to herein as the pinned triple line phase), where the evaporation loss is accommodated by a decreasing contact angle with the solid-liquid interface area remaining constant; a second phase involving a constant contact angle (referred to herein as the moving triple line phase) with a decrease in the contact area and the third phase where a mixed behavior was observed. They also proposed that the switching of the evaporation to the second

phase occurs at the point where the droplet reaches a contact angle equal to the θ_r for that surface. Later, Birdi and co-workers [2, 4] studied the behavior of water and n-octane drops placed on smooth surfaces of glass and Teflon®. They concluded that the constant contact area phase could be expected for wetting drops (θ <90) and the constant contact angle phase is more likely to occur with non-wetting drops (θ >90). This study did not consider the effect of surface topology and chemical composition of these surfaces. It has since been shown that whether a drop evaporates following either of these two methodologies depends more significantly on the contact angle hysteresis than on the absolute value of the contact angle [5]. In other words, the drop will continue to evaporate in the pinned TL phase as long as the instantaneous contact angle is greater than the θ_r.

Shanahan and Bourges [6] studied evaporation of water and n-decane drops on various substrates ranging in 'roughness' and evaporating under varying atmospheric conditions. They observed the evaporation characteristics of a water drop in both closed and open systems from which they concluded that the evaporation occurs in four stages - The first stage corresponding to a saturated atmosphere and the remaining evaporation process to occur in two or three phases depending on the surface roughness. Stage II was observed to be with a constant contact area. Stage III was observed for smooth surfaces in which the drop height and contact radius were observed to diminish keeping the contact angle constant. This stage was observed to be absent for rough surfaces. Stage IV was corresponding to the final drop disappearance. The results also emphasized the importance of atmospheric conditions in contact angle measurements, an issue that was seemingly overlooked in the earlier literature. McHale et al. [7] investigated the effect of surface topology on the evaporation process. Their experiments showed that the water droplets initially evaporated with a constant contact area before the triple line receded in a stepwise fashion jumping from pillar to pillar corresponding to the Cassie-Baxter state [8]. In some cases, the droplet was observed to collapse into the pillar structure abruptly with further evaporation occurring with completely pinned contact area consistent with a Wenzel type state [9]. The recent review article by Plawsky et al. [10] presents a detailed review of the state of the art in this regard.

A significant amount of the literature suggests that understanding evaporation phenomenon requires the knowledge of wetting properties of the surfaces, in particular, the wetting hysteresis that can be defined as the difference between θ_a and θ_r. Soolaman et al. [11] observed that the evaporation phase switching was found to be independent of surface wettability but yet correlated with the wetting hysteresis [12]. The evaporation rate was found to increase with the greater hydrophilic nature of the surface, owing to the decreased instantaneous contact angle and the increased surface area per unit volume [13, 14]. Studies of evaporation on rough substrates is advantageous in that both pinned and moving TL phases can be observed, one following the other, in the same experimental test. As a result, direct comparison of the rates of evaporation is feasible.

The wettability of an ideal surface can be characterized by a single contact angle, viz. the Young's angle which is determined by Gibbs free energy minimization process. The rate of evaporation is known to depend on the contact angle [2]. However on a real surface, the instantaneous quasistatic contact angle can take on a value between two limiting values, owing to the phenomenon of defect pinning [15]. We have recently shown that for rough substrates, the defect pinning phenomenon is only activated in cases where the triple line is continuous [16]. The triple line was observed to be discontinuous for surfaces with pillars. This is for the reason that, the triple line, defined as the set of points in contact with the solid, liquid and vapor phases, is in the form of loops around the edges of the top of the pillars [16]. Since wettability and evaporation processes are intricately linked, and since the macroscopic contact angle that characterizes wettability depends on the microscopic triple line topology, it is conceivable that the evaporation is also affected by the triple line topology. In other words, we consider herein the effect of the fact that the triple line is either continuous or discontinuous on the evaporation of liquid from a sessile drop. As Anantharaju et al. [16] have shown, the triple line on a substrate with etched square holes is continuous while a substrate with square pillars would manifest a discontinuous triple line. We herein present experiments to study the effect of this triple line topology on the nature of evaporation and transition from a pinned triple line phase to a moving triple line phase.

Experimental procedure

The evaporation rate constant of a sessile drop is characterized by measuring the dynamic contact angles as well as the solid-liquid contact area during evaporation. The specimens used during this test program consisted of periodically placed square pillars as well as square holes. These specimens had heterogeneity length scale, a (side of the square feature) varying between 5 and 100μ and solid area fraction, f varying between 25% and 75%. Here f is defined as the solid-liquid contact area per unit total area (see figure 2). The specimens were fabricated by photolithography process of silicon wafers and silanized for hydrophobicity [16]. Table 1 indicates the characteristics associated with the set of specimens used during this test process. For example, H_a20_f75 refers to a specimen consisting of holes type topology with heterogeneity length scale, a=20μ and 75% solid area fraction. Similarly, P_a50_f50 refers to a specimen with pillars type of topology with heterogeneity length scale, a=50μ and of 50% solid area fraction. For the values not reported in table 1, it was difficult to obtain repeatability. Details of the specimen and fabrication procedure can be found in Anantharaju et al. [16] The sessile droplet was carefully placed on the specimen such that the drop was in the Cassie state and the initial contact angle being equal to the θ_a of the surface. A contact angle goniometer mounted on vibration-free table, was used to capture the evaporation process by acquiring static images of the drop at a two minute interval. These images are subsequently post processed to obtain the instantaneous contact angle, θ, and the instantaneous contact circle radius, r, during the evaporation process. The instantaneous drop volume was calculated from the measured values of r and θ. The ambient temperature and water vapor concentration in the lab were measured using a type J thermocouple and an RH meter, respectively. The relative humidity in the lab as well as the ambient temperature was noted at periodic intervals during the evaporation process. At least two trials were performed on each specimen. The table 1 reports the average values of dimensionless evaporation rate constants and contact angles on each of the specimens.

Results and Discussion

The results obtained from an experimental study of an evaporating sessile water drop placed on a test specimen with the just advanced angle are presented herein. A set of such evaporation experiments were performed on a series of substrate specimens in order to identify the effect of surface characteristics on the evaporation rate constant. Qualitatively, the evaporation process was observed to occur in four phases (see selected images presented in figure 3. These images are selected from a full time series obtained on specimen H_a20_f25). During the first phase, the atmosphere in the vicinity of the sessile drop is allowed to reach a state of saturation. This phase occurs over a very short duration in time and is not shown in figure 3. In the second phase, referred to as the pinned TL phase, the contact area of the drop with the solid surface remains unchanged. During this phase, the contact angle was observed to decrease to accommodate the decrease in the drop volume. In the third phase of evaporation, the moving TL evaporation phase, the contact angle remained constant while the contact area decreased continuously. In several of the data runs, the final two images of the data series demonstrated a fourth phase where both the contact area as well as the drop contact angle decreased rapidly (approaching zero). We herein refer to this phase as the mixed phase, but do not report results, as these measurements (involving drops of very small volume, e.g. figure 3j) are prone to measurement error.

The contact angle manifested by the drop during phase II decreased until the receding angle, θ_r of the surface was reached (see figure 3a-d). The constant contact angle observed in phase III was equal to this θ_r. This observation was also confirmed through independent measurements of θ_r on that surface using the conventional volume withdrawal method [16]. At this point in time, the evaporation process changes to the moving TL phase (see figure 3e-h) [17]. In both the phases II and III, the drop evaporation was observed to independently satisfy the D^2 law [18, 19], according to which,

$$[D(t)]^2 = D_0^2 - K't \quad (1)$$

Here D is the diameter of the spherical cap as a function of time, t. D_o is the initial diameter of the spherical cap for each phase of evaporation. K' (m^2/s) is termed the evaporation rate constant. This value was found to be different during the pinned (K'_p) and moving (K'_m) triple line phases. The value of the evaporation rate constant depends on the ambient temperature and humidity, which were observed to vary trial to trial. In order to isolate the effects of the surface characteristics on evaporation rate constant, these values need to be non-dimensionalized. The calculated evaporation rate constants associated with the sessile drop evaporation process were non-dimensionalized with the theoretical evaporation rate constant of a spherical drop, K'_s evaporating under the same temperature and humidity conditions. For such a spherical drop, the evaporation rate constant, K'_s is given by [18],

$$K'_s = \frac{8\rho\alpha_w \ln(1+B_Y)}{\rho_l} \tag{2}$$

Here α_w is the diffusivity of water vapor in air and B_Y is the dimensionless transfer number given by

$$B_Y = \frac{C_R - C_\infty}{1 - C_R} \tag{3}$$

Both α_w and B_Y are dependent on the ambient temperature as follows. C_R , which is the saturation water vapor concentration, is measured during the course of the experiment. C_∞ , the ambient water vapor concentration is obtained from psychrometric chart using the measured ambient temperature. The value of α_w at that ambient temperature (T) is estimated using [18],

$$\frac{\alpha_w(T)}{\alpha_w(273K)} = \left(\frac{T}{273}\right)^{3/2} \tag{4}$$

where α_w at 273K is 2.2×10^5 m^2/s. Finally ρ_l is the liquid density and ρ is the density of the moist air, which is again calculated from the known ambient temperature and relative humidity.

Figure 4 is a plot of $V^{(2/3)}$ (effectively D^2) varying with time for a smooth silanized surface and two rough surfaces: P_a20_f50 and H_a20_f50. It may be noted that both these specimens are of the same heterogeneity length scale and solid area fraction. The evaporation data presented in figure 4

independently obey equation (1) for both the pinned and moving TL phases [20]. It is possible to calculate the dimensional evaporation rate constant (K_P' and K_m') from a least squares fit of each series presented in this graph. However it is not possible to isolate the effect of the surface topology from these dimensional evaporation rate constants, due to the fact that this data was obtained under different ambient conditions (on different days) and therefore at different values of transfer numbers, B_Y and α_w. The evaporation rate constants obtained as the slope of the data presented in this figure need to be non-dimensionalized by K_s' calculated from equation (2) using the B_Y and α_w corresponding to the conditions measured during each experiment. The dimensionless evaporation rate constants can then be used to isolate the effect of the surface and triple line topology on the evaporation process.

The transition point from phase II to phase III needs to be identified in order to calculate the dimensional K_p' and K_m' values. This transition point in each experiment is identified from a plot similar to figure 5. Figure 5 shows the contact angles (represented by open symbols) and the contact circle diameters, 2r, (represented by solid symbols) varying with time for the smooth (S) and rough surface (H_a20_f50) used to generate the data in figure 4. The two phases of evaporation, viz. pinned TL phase (where the contact circle diameter is constant) and the moving TL phase (where the contact angle is constant) can be clearly observed from this figure. For example, for the smooth surface, this transition is observed to occur at a time of 3120s. A least squares linear fit to obtain the slope of the $V^{(2/3)}$ versus t data for $0<t<3210$ would yield K_p' and a similar fit for $3120<t<4200$ would yield K_m'. It may be noted that for t>4200, the evaporation is observed to transition to a mixed phase. It was observed that the values of K_p' and K_m' were reproducible within 5.3% and 8.3% respectively. Finally, these dimensional evaporation rate constant values are rendered dimensionless using K_s' from equation (2) such that

$$K_p = \frac{K_p'}{K_s'} \tag{5}$$

and

$$K_m = \frac{K'_m}{K'_s} \tag{6}$$

The dimensionless K_p and K_m values for surfaces with holes and pillars varying in solid area fraction and heterogeneity length scales are presented in table 1. An example non-dimensionalization calculation and the complete raw data set is included in the supplementary information section. Firstly, the values of K_m are observed to be higher than the K_p values for all the surfaces. This is explained by the fact that the pinned TL phase evaporation occurs with the drop contact angle gradually decreasing from the θ_a to θ_r, whereas, the moving TL phase of evaporation occurs at a constant value of the drop contact angle equal to θ_r. Soolaman et al. [11] have shown an inverse correlation between the evaporation rate constant and contact angle. Since the average contact angle during the pinned TL phase is higher than the average contact angle in the moving TL phase, the evaporation rate constant in the pinned TL phase is expected to be lower than that in the moving TL phase. This is a direct consequence of lower contact angles producing greater surface area per volume [21].

Figure 6 is a plot of the K_p versus the initial contact angle during the pinned TL phase. A trend line is presented in this figure only to indicate the qualitative behavior in the data. It may be recalled, that the initial angle of the sessile drop at the start of the pinned TL phase evaporation is chosen to be θ_a. The θ_a on a smooth silanized surface was measured to be 103° and it is known that roughness amplifies hydrophobicity [22] which is characterized by an increase in the contact angles. It can be observed from figure 6 that as the initial angle increases, the pinned TL evaporation rate constant decreases. Figure 7 is a plot similar to figure 6 for K_m versus the constant contact angle during the moving TL phase, i.e. the θ_r. This graph depicts a qualitative trend similar to figure 6 that the evaporation rate constant decreases with increasing contact angle [13].

Further, we study the energy barriers associated with the stick-slip motion of the drop during the evaporation process. Figure 8 shows the variation of the contact angle and contact radius during the sessile drop evaporation process on a substrate with square pillars of side 100μ and 25% area fraction

(spacing between the centers of the pillars = 200 μ). The data points on this figure are taken at two minute intervals. The circled points on this figure for the base radius represent the individual stick-slip events. From this figure it can be observed that, in the pinned TL phase, the TL remains pinned with the decrease in the volume during evaporation being accomodated by a corresponding decrease in the contact angle till the receding angle of the surface is reached. Further, the first stick-slip event can be observed to coincide with the transition of the evaporation process from phase II to phase III. Further, motion of the TL during phase III was observed to have multiple such stick-slip events.The energy barrier per unit length of the TL associated with this stick-slip event is given by [23],

$$\delta G \approx \frac{\gamma \sin^2 \theta_r (2+\cos \theta_r)(\delta r)^2}{2r} \quad (7)$$

Here, γ is the surface tension of the evaporating liquid, θ_r is the receding angle of the surface calculated as the constant angle with which the triple line recedes in phase III, δr is the slipped distance local to the stick-slip event, and r is the local pinned TL radius before the TL slips. The energy barriers were estimated following Shanahan [23] for each of the stick-slip events in figure 8. Two significant conclusions can be drawn from this study,

(i) The average slip distance for all the stick-slip events (205μ) was remarkably close to the spacing between the centers of the pillars for that surface.

(ii) The average energy barrier per unit length of the TL from equation (7) was calculated to be 2.23×10^{-6} N which is of the same order of magnitude as other triple line tension measurements reported in the literature [24].

We next investigate the effect of contact line topology (continuous verus discontinuous) on the evaporation process. From table 1, consider the substrates with microscale roughness of square holes (H_a50_f75) and square pillars (P_a50_f75). These two surfaces have similar θ_a and θ_r values for the same heterogeneity length scale of 50μ and solid area fraction of 75%. The only difference in the two surfaces is in the triple line topology which is observed to be continuous for H_a50_f75 and

discontinuous for P_a50_f75. The K_p values (0.43, and 0.45) and K_m values (0.5 and 0.53) for these two specimens (H_a50_f75 and P_a50_f75 respectively) can be observed to be similar. The surfaces with square pillars producing discontinuous triple lines have larger surface area of the drop exposed for evaporation in comparison with that of square holes. For this reason, the evaporation rate constants on these surfaces are expected to be higher. But from comparing the K_p and K_m values for the surfaces under consideration, it can be concluded that the evaporation rate constants on surfaces are not affected by the triple line topology.

Conclusions

Sessile drop evaporation on smooth and rough surfaces was studied experimentally. Four distinct phases of evaporation were observed: (i) saturation phase, (ii) pinned triple line phase, (iii) moving triple line phase and (iv) mixed phase. The evaporation rate constant in the pinned and moving triple line phases was calculated from measurements of drop volume versus time for surfaces with roughness varying in heterogeneity length scales and solid area fractions as well as triple line topology. The evaporation rate constant is known to vary with ambient temperature and humidity. Since the experiments were done at different temperatures and relative humidities, the dimensional evaporation rate constant is non-dimensionalized using the theoretical evaporation rate constant for a spherical drop evaporating under the same conditions. This non-dimensionalization process thus helps us isolate the effect of the surface characteristics. The dimensionless evaporation rate constant was observed to be higher on a smooth surface in comparison to rough surfaces. This is shown to be due to the fact that roughness amplifies the surface hydrophobicity characteristics and hence causes a higher average contact angle during the evaporation process. Finally, the evaporation rate constant was observed to be higher in the moving triple line phase in comparison with that in the pinned triple line phase due to higher contact angles during the pinned triple line phase. Also, the triple line topology was observed to not affect the evaporation rate constant values. Further, a calculation of the energy barriers associated with the stick-slip motion of the drop showed that the slip distance was of the order of the center spacing between the

pillars and that the energy barrier was of the same order of magnitude as the line tension reported in the literature.

ACKNOWLEDGMENT: We thank the Department of Energy EERE for partially supporting the work presented herein. The help of Mr. Wayne Kimsey in developing the software for image analysis is greatly appreciated. Finally, the help of CESR at TTU is appreciated for all their support during this research project.

FIGURES:

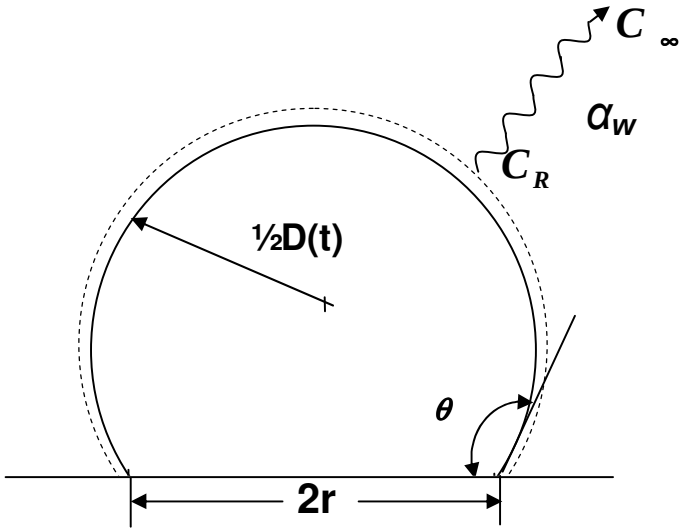

Figure 1: Schematic of sessile drop evaporation

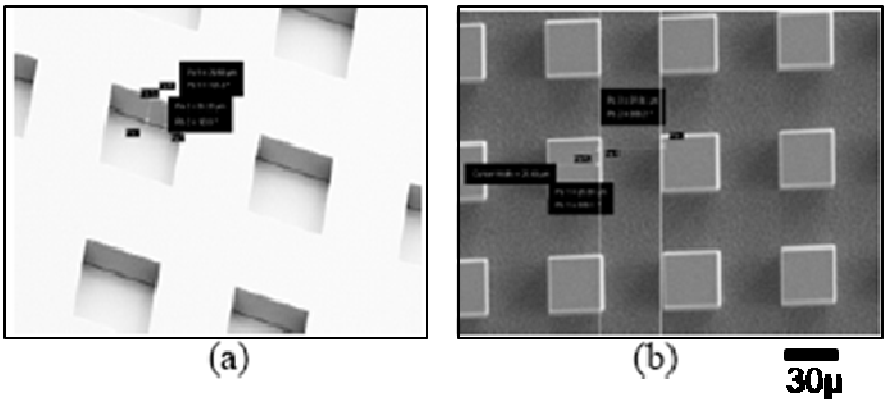

Figure 2: SEM images of the specimen with (a) square holes and (b) square pillars (bar=30μ)

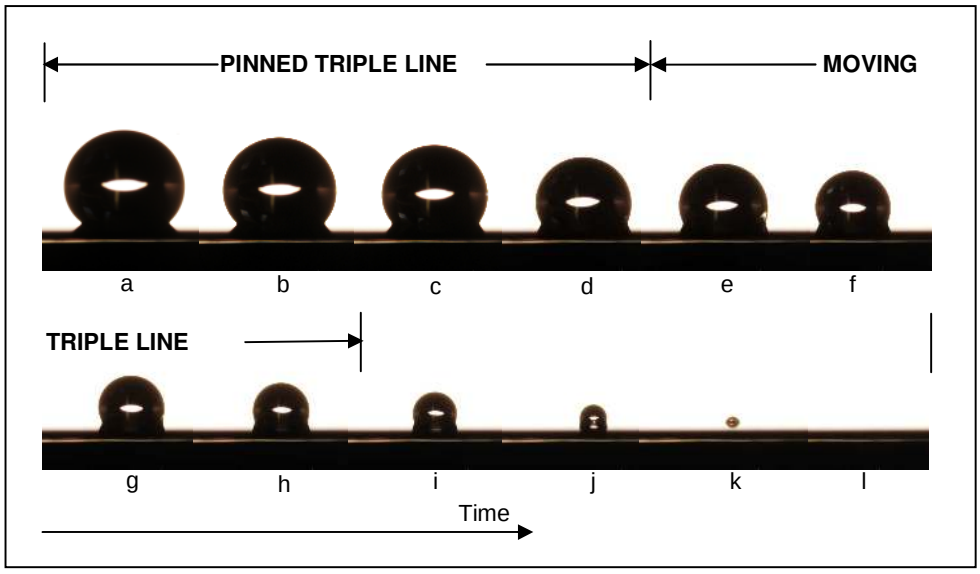

Figure 3: Drop evaporation in the pinned and moving triple line phases

.

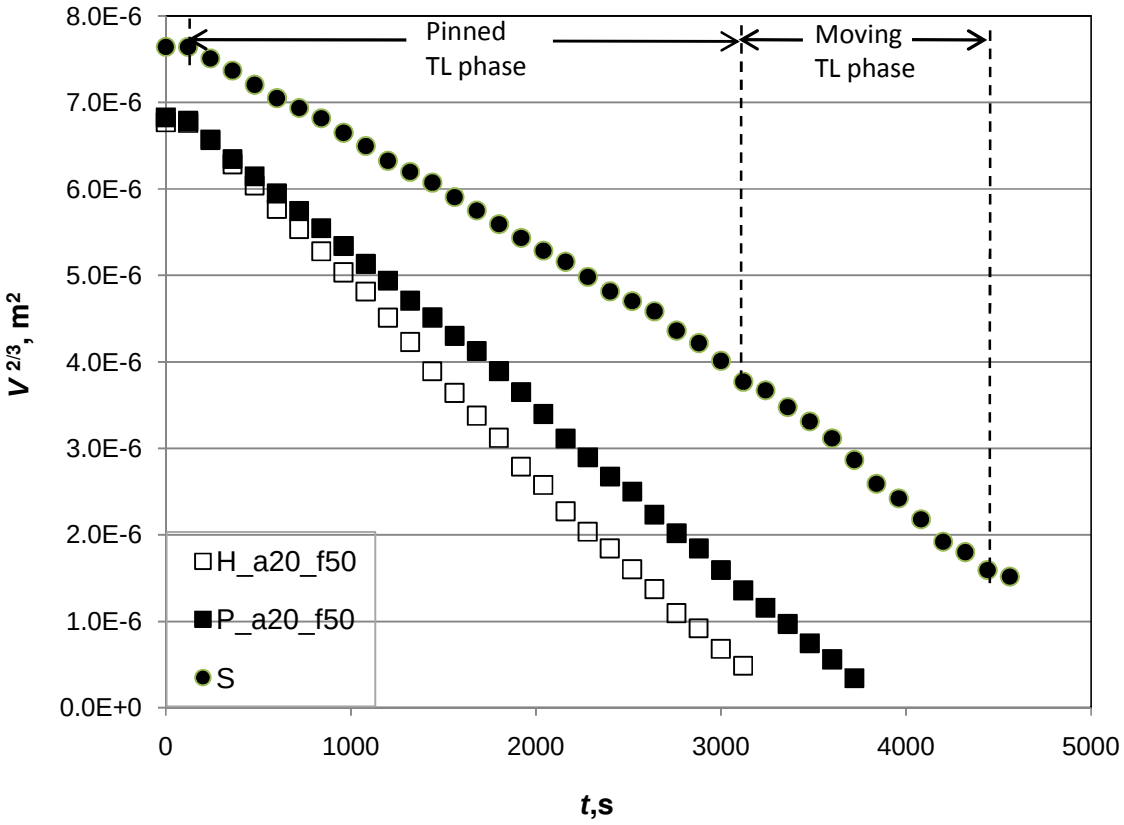

Figure 4: $V^{2/3}$ varying with time on a silanized smooth surface and surfaces with holes and pillars.

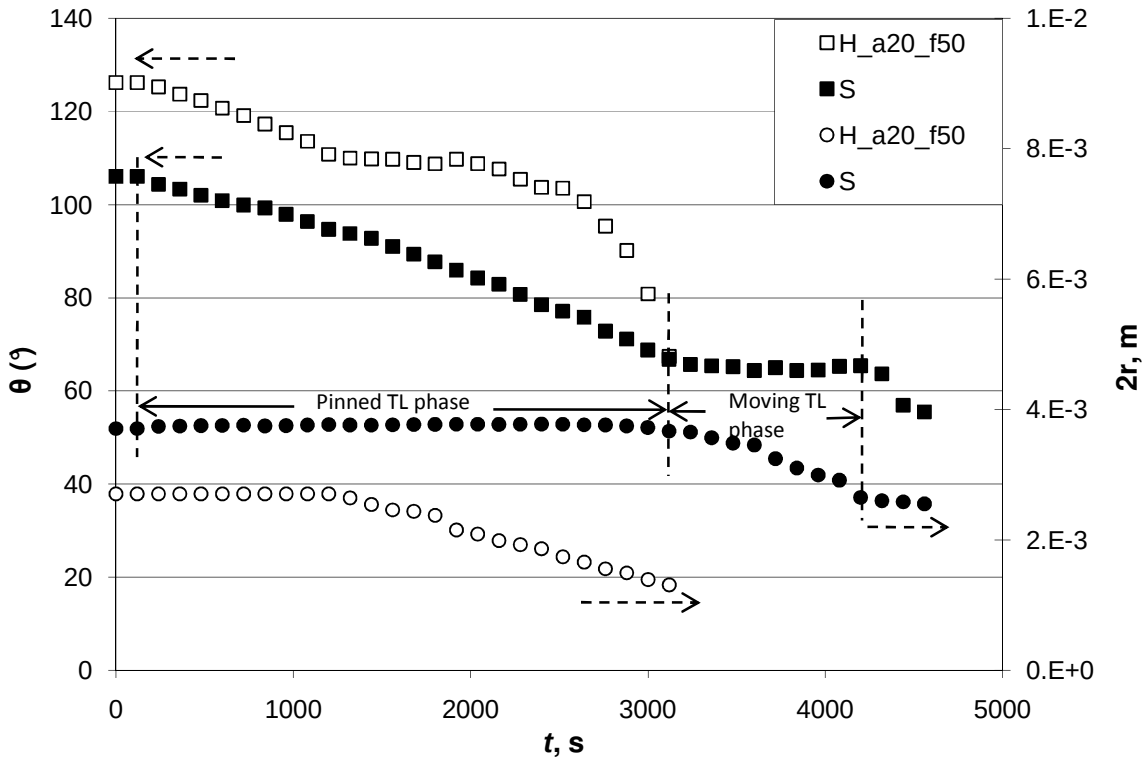

Figure 5: Contact angles and contact circle diameters varying with time for a smooth surface and a surface with holes

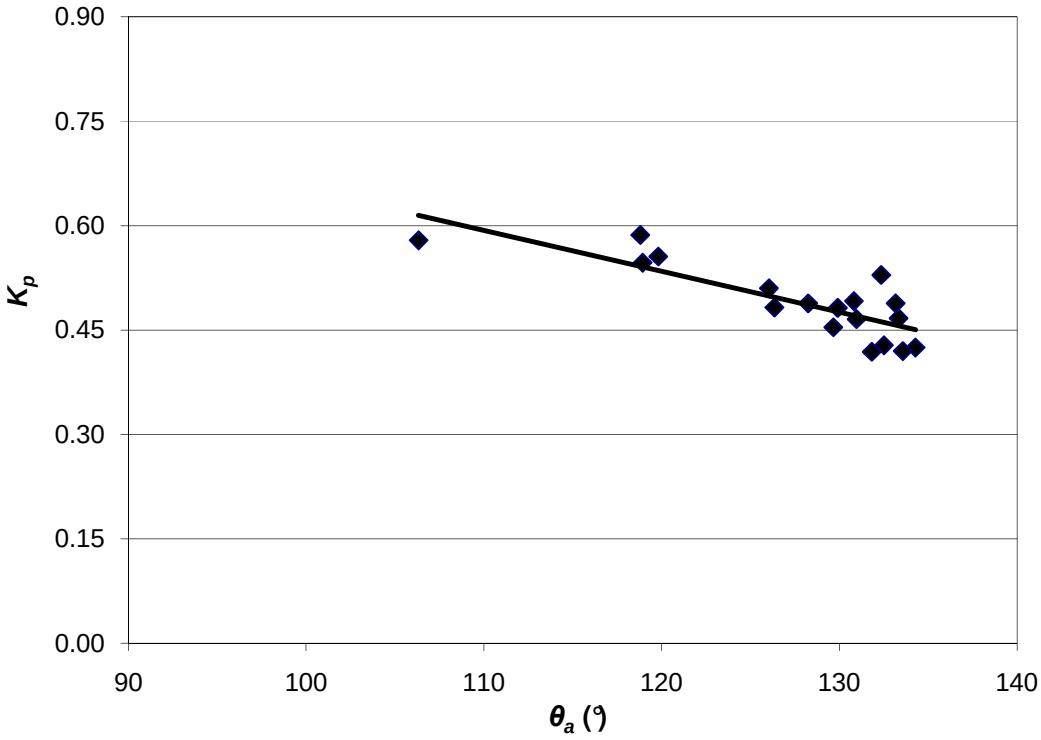

Figure 6: Dimensionless K_p values varying with the initial contact angle (advancing contact angle of the drop). {Least squares regression co-efficient, R^2=0.67}

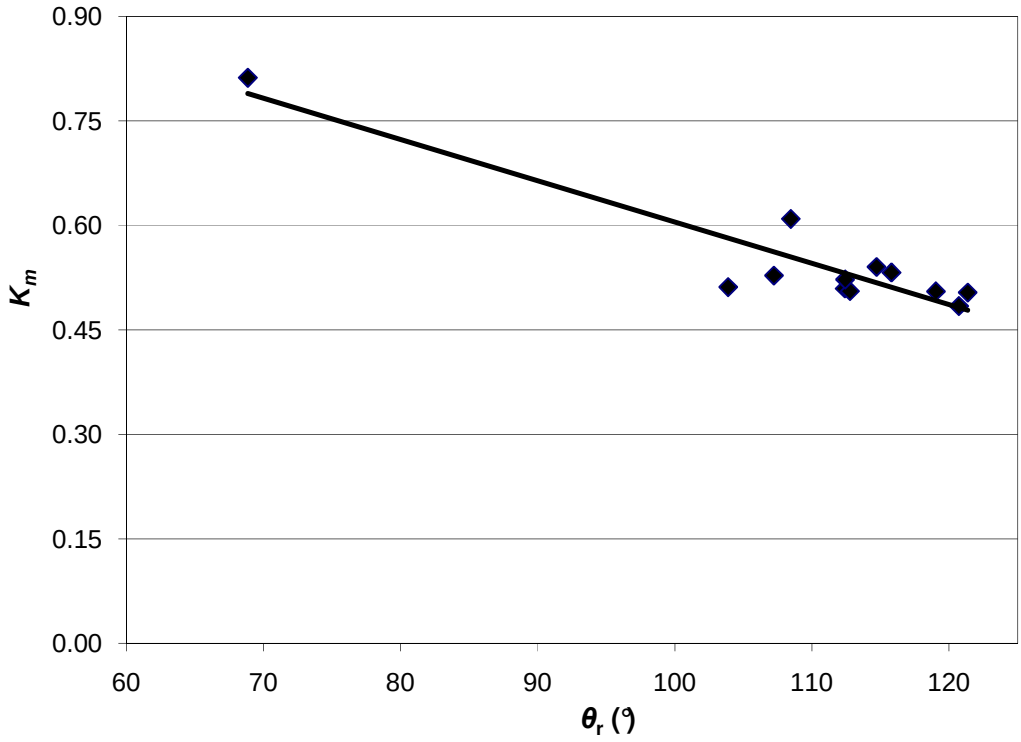

Figure 7: Dimensionless K_m values varying with the constant contact angle in moving TL phase (receding contact angle of the drop). {Least squares regression co-efficient, R^2=0.86}

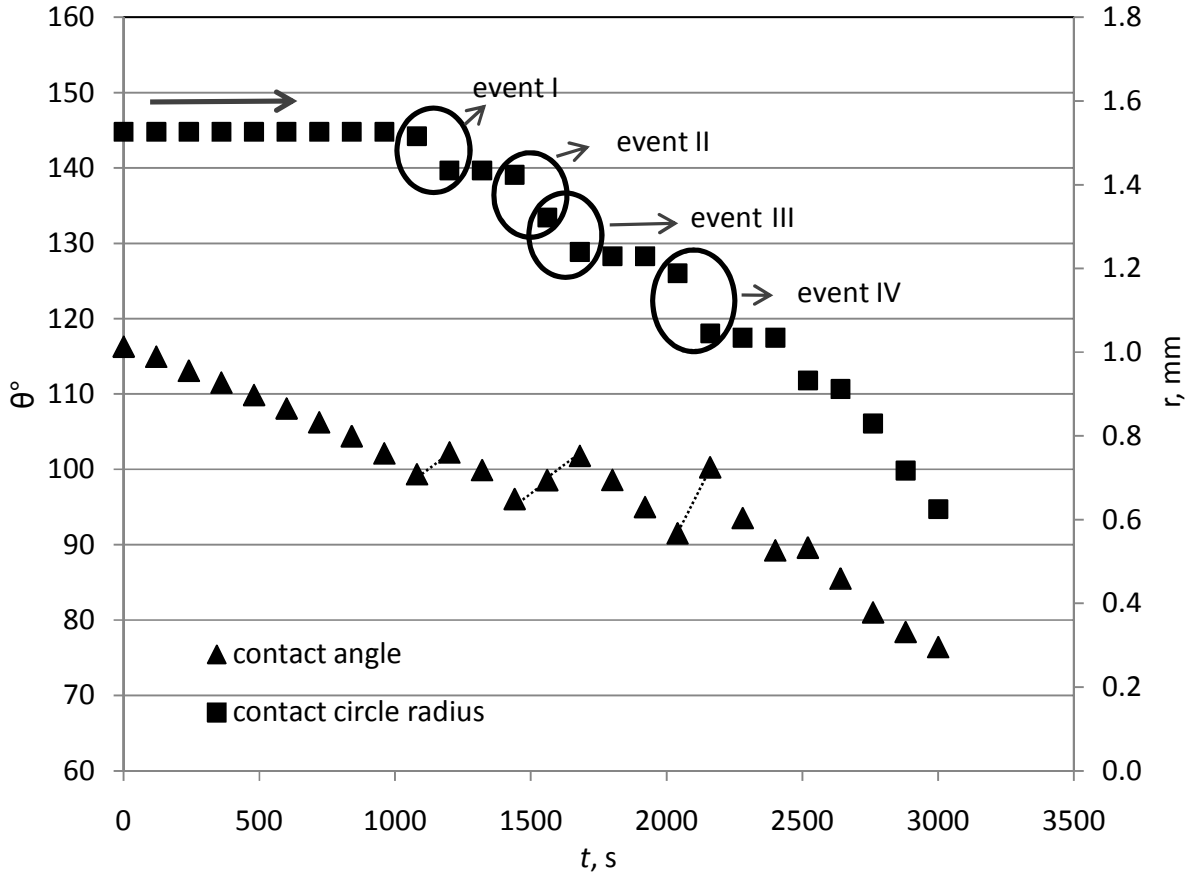

Figure 8: Contact angle and contact circle radius varying with time during the evaporation process on a surface with pillars with center spacing of 200μ and with 25% area fraction.

Specimen ID	Surface topology	a, μ	Solid area fraction, f	K_p	K_m	θ_a	θ_r
H_a5_f50	Hole	5	0.5	-	0.54	-	114.7
H_a5_f75	Hole	5	0.75	0.42	0.48	134.3	120.7
H_a10_f50	Hole	10	0.5	-	0.51	-	112.4
H_a20_f50	Hole	20	0.5	0.47	0.52	133.4	112.4
H_a20_f75	Hole	20	0.75	-	0.5	-	121.4
H_a50_f25	Hole	50	0.25	0.49	-	130.8	-
H_a50_f50	Hole	50	0.5	0.53	-	132.4	-
H_a50_f75	Hole	50	0.75	0.43	0.5	132.5	119.1
H_a100_f25	Hole	100	0.25	0.49	-	133.2	-
H_a100_f50	Hole	100	0.5	0.41	-	131.8	-
P_a3_f25	Pole	3	0.25	0.59	-	118.8	-
P_a5_f0.25	Pole	5	0.25	0.55	-	118.9	-
P_a5_f0.5	Pole	5	0.5	0.51	-	126.4	-
P_a10_f0.5	Pole	10	0.5	0.48	0.51	129.9	103.9
P_a20_f0.25	Pole	20	0.25	-	0.61	-	108.5
P_a20_f0.5	Pole	20	0.5	0.48	0.52	126.4	107.2
P_a20_f0.75	Pole	20	0.75	-	0.5	-	112.8
P_a50_f0.5	Pole	50	0.5	0.49	-	128.3	-
P_a50_f0.75	Pole	50	0.75	0.45	0.53	129.7	115.8
P_a100_f0.25	Pole	100	0.25	0.55	-	119.8	-
P_a100_f0.5	Pole	100	0.5	0.46	-	131.0	-
P_a100_f0.75	Pole	100	0.75	0.41	-	133.6	-
S (smooth surface)				0.58	0.81	106.3	68.9

Table 1: Dimensionless K_p and K_m values for surfaces with pillars and holes of different heterogeneity length scales and solid area fractions.

REFERENCES

1 Gokhale, S.J., Plawsky, J.L. and Wayner, P.C., *Spreading, evaporation and contact line dynamics of surfactant laden microdrops,* Langmuir, 2005, **21**, p: 8188-8197.

2 Birdi, K.S. and Vu, D.T., *Wettability and the evaporation rates of fluids from solid surfaces*, J. Adhesion Sci. Technol., 1993, **7**(6), p: 485-493.

3 Picknett, R.G. and Bexon, R., *The evaporation of sessile or pendant drops in still air*, J. Colloid Interface Sci., 1997, **61**(2), p: 336-350.

4 Birdi, K.S., Vu, D.T. and Winter, A., *A study of the evaporation rates of small water drops placed on a solid surface*, J. Phys. Chem., 1989, **93**, p: 3702-3703.

5 Extrand, C.W., *Contact angles and hysteresis on surfaces with chemically heterogeneous islands*, Langmuir, 2003, **19**(9), p: 3793-3796.

6 Bourges-Monnier, C. and Shanahan, M.E.R., *Influence of Evaporation on Contact Angle,* Langmuir, 1995, **11**, p: 2820-2829.

7 McHale, G., Aqil, S., Shirtcliffe, N.J., Newton, M.I. and Erbil, H.Y., *Analysis of droplet evaporation on a superhydrophobic surface,* Langmuir, 2005, **21**(24), p:11053-11060.

8 Cassie, A.B.D., *Contact angles,* Discussions of the Faraday Society, 1948, **3**.

9 Amirfazli, A., Kwok, D.Y., Gaydos, J. and Neumann, A.W., *Line tension measurements through drop size dependence of contact angle,* J. Colloid Interface Sci., 1998, **205**, p:1-11.

10 Plawsky, J.L., Ojha, M., Chatterjee, A. and Jr. Wayner, P.C., *Review of the effects of surface topology, surface chemistry, and fluid physics on evaporation at the contact line,* Chemical Engineering Communications, 2009, **196**(5), p: 658 — 696.

11 Soolaman, D.M. and Yu, H.Z., *Water microdrops on molecularly tailored surfaces: correlation between wetting and evaporation mode switching,* J. Phys. Chem., 2005, **109**, p:17967-17973.

12 Yu, H.Z., *Evaporation of water microdroplets on self-assembled monolayers: From pinning to shrinking,* J. Chem. Phys., 2004, **5**, p:1035-1038.

13 Deegan, R.D., Bakajin, O., Dupont, T.F., Huber, G., Nagel, S.R. and Witten, T.A., *Capillary Flow as the cause of ring stains from dried liquid drops*, NATURE, 1997, **389**, p:827-829.

14 Deegan, R.D., Bakajin, O., Dupont, T.F., Huber, G., Nagel, S.R. and Witten, T.A., *Contact line deposits in an evaporating drop,* Phys. Rev. E, 2000, **62**(1), p:756-765.

15 de Gennes, P.G., *Wetting: statics and dynamics,* REVIEWS OF MODERN PHYSICS, 1985, **57**(3), p:827-863.

16 Anantharaju, N., Panchagnula, M.V., Vedantam, S., Neti, S. and Tatic-Lucic, S., *Effect of three-phase contact line topology on dynamic contact angles on heterogeneous surfaces*, Langmuir, 2007, **23**, p: 11673-11676.

17 Kim, J.-H., Ahn, S.I., Kim, J.H. and Zin, W.-C., *Evaporation of water droplets on polymer surfaces,* Langmuir, 2007, **23**, p: 6163-6169.

18 Turns, S.R., *An introduction to combustion*.

19 Meric, R.A. and Erbil, H.Y., *Evaporation of sessile drops on solid surfaces: Pseudospherical cap geometry,* Langmuir, 1998, **14**, p:1915-1920.

20 Erbil, H.Y., McHale, G., and Newton, M. I., *Drop Evaporation on Solid Surfaces: Constant Contact Angle Mode*, Langmuir, 2002, **18**, p: 2636-2641.

21 Extrand, C.W., *Relation between contact angle and the cross-sectional area of small, sessile liquid drops,* Langmuir, 2006, **22**, p: 8431-8434.

22 Wenzel, R.N., *Resistance of solid surfaces to wetting by water*, Industrial & Engineering Chemistry, 1936, **28**(8), p: 988-994.

23 Shanahan, M.E.R., *Simple theory of "stick-slip" wetting hysteresis,* Langmuir, 1995, **11**(3), p: 1041-1043.

24 Neumann, A.W. and Good, R.J., *Thermodynamics of Contact Angles. I. Heterogeneous Solid Surfaces*, J. Colloid Interface Sci., 1972, **38**, p:341-358.